Supporting Information:

Core-shell PdAu nanocluster catalysts to suppress sulfur poisoning

Shan Gao[a,b], Linxia Wang[a], Hui Li[a], Zunfeng Liu[b], Guoliang Shi[c], Jianfei Peng[d], Bin Wang[e], Weichao Wang[a,*], Kyeongjae Cho[f]

[a] *Integrated Circuits and Smart System Lab (Shenzhen), Renewable Energy Conversion and Storage Center, Tianjin Key Laboratory of Photo-Electronic Thin Film Device and Technology, College of Electronic Information and Optical Engineering, Nankai University, Tianjin, 300071, China*

[b] *State Key Laboratory of Medicinal Chemical Biology, College of Pharmacy, Nankai University, Tianjin, 300071, China*

[c] *State Environmental Protection Key Laboratory of Urban Ambient Air Particulate Matter Pollution Prevention and Control, Tianjin Key Laboratory of Urban Transport Emission Research, College of Environmental Science and Engineering, Nankai University, Tianjin, 300350, China*

[d] *Tianjin Key Laboratory of Urban Transport Emission Research, College of Environmental Science and Engineering, Nankai University, Tianjin, 300071, China*

[e] *Shenzhen Key Laboratory of Advanced Thin Films and Applications, College of Physics and Optoelectronic Engineering, Shenzhen University, Shenzhen, 518060, China*

[f] *Department of Material Science and Engineering, University of Texas at Dallas, Richardson, 75080, USA*

* *Corresponding Author*

E-mail: weichaowang@nankai.edu.cn

Contents

Supplementary details of MC simulations

Monte Carlo simulations were performed using the embedded atom method (EAM) potential. We tested the functions and parameters provided in the literature of Zhou et al.[s1], Shan et al.[s2-3] and Marchal et al.[s4] Table S1 shows the DFT and EAM calculated lattice constants (Å) and cohesive energies (eV) of bulk Pd_xAu_y (x + y = 4) systems. Both the parameters refer to the Shan et al. and Marchal et al. articles reproduced reasonable results for bulk PdAu systems. We checked the MC simulation results based on different EAM parameters and found it had the same accepted configuration for the studied nanoparticles. The cohesive energy of a system is defined as

$$E_{coh}^{DFT} = \frac{1}{n}\left[E^{DFT}(Pd_xAu_y) - xE^{DFT}(Pd) - yE^{DFT}(Au)\right]$$

$$E_{coh}^{EAM} = \frac{1}{n}E^{EAM}(Pd_xAu_y)$$

where E_{coh}^{DFT} refers to the DFT calculated cohesive energy, $E^{DFT}(Pd_xAu_y)$ is the DFT energy of the system, and $E^{DFT}(Pd)$ and $E^{DFT}(Au)$ are the DFT atomic energies of the Pd and Au atoms, is defined as divided the energy of corresponding metal bulk by atom number; E_{coh}^{EAM} refers to the EAM calculated cohesive energy, $E^{EAM}(Pd_xAu_y)$ is the EAM energy of the system.

Table S1 The DFT and EAM calculated lattice constants (Å) and cohesive energies (eV) of the bulk PdAu systems.

	a_{DFT}	a_{EAM}			E_{coh}^{DFT}	E_{coh}^{EAM}		
		Zhou [s1]	PRB [s2-3]	JPCC [s4]		Zhou [s1]	PRB [s2-3]	JPCC [s4]
Pd	3.95	3.890	3.955	3.972	-3.71	-3.909	-3.71	-3.70
Pd_3Au	4.01	3.938	4.016	4.004	-3.57	-3.944	-3.59	-3.61
PdAu	4.06	3.986	4.071	4.052	-3.42	-3.959	-3.43	-3.45
$PdAu_3$	4.12	4.032	4.124	4.119	-3.24	-3.953	-3.23	-3.23
Au	4.17	4.080	4.172	4.190	-2.99	-3.930	-2.99	-2.99

Information for molecules adsorption

Table S2 The adsorption energies and geometric data at all the possible non-equivalent binding sites for the adsorption of SO_2 on the Pd_{55} cluster. The subscripts of element symbol represent their actual binding sites on the cluster, V is short for the vertex site, E is short for the edge site, B1 is short for the bridge site between vertex and edge atoms and B2 is short for the bridge site between two edge atoms, F represents fcc hollow and H represents hcp hollow. The most favorite configuration is in bold letters.

Adsorption site		d_{S-M}/ Å	d_{O-M}/ Å	d_{S-O}/ Å	∠O-S-O/ °	Adsorption energy/ eV
Initial	Final					
S_V	-	2.147		1.454,1.454	118.169	-1.09
S_E	-	2.212		1.468,1.467	117.489	-1.05
S_VO_E	-	2.229	2.132	1.470,1.527	114.733	-1.43
S_EO_E	$S_{B1}O_E$	2.236,2.230	2.298	1.458,1.510	114.163	-1.79
$S_{B2}O_V$	**-**	2.240,2.234	2.216	1.459,1.518	113.140	**-1.96**
$S_{B2}O_E$	-	2.240,2.237	2.296	1.461,1.509	113.339	-1.74
$S_VO_EO_E$	-	2.226	2.185,2.187	1.521,1.521	112.175	-1.70
$S_EO_EO_E$	-	2.239	2.197,2.198	1.521,1.521	110.794	-1.57

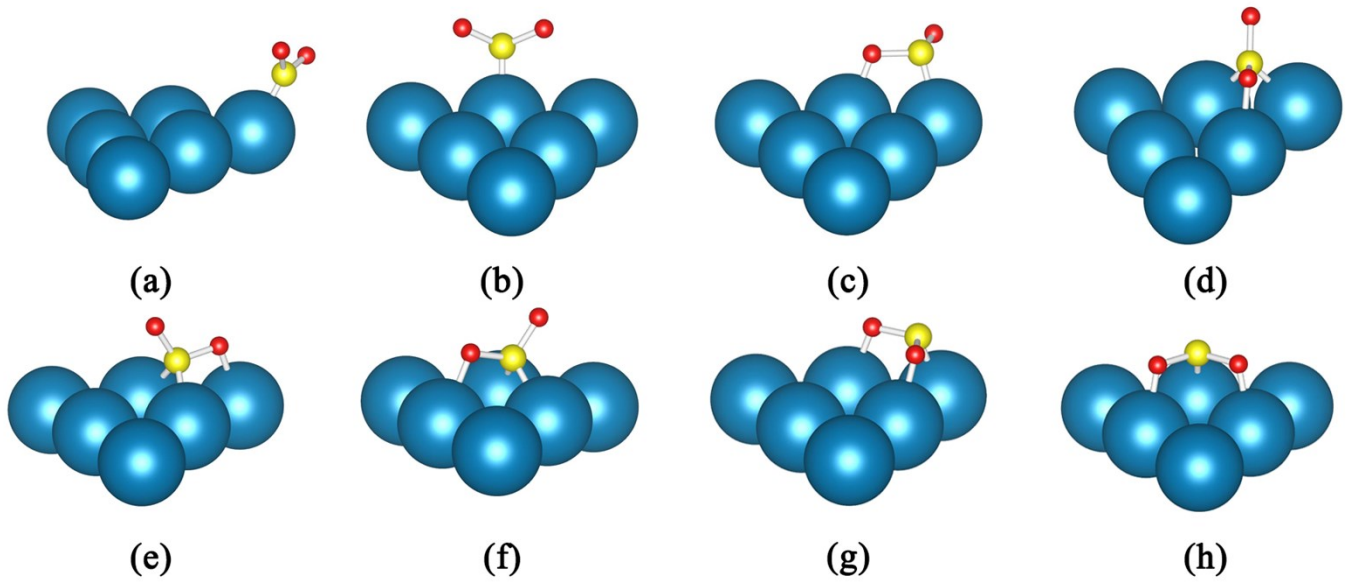

Figure S1 The optimized adsorption configurations at all the possible non-equivalent binding sites for the adsorption of SO_2 on the Pd_{55} cluster.

Table S3 The adsorption energies and geometric data at all the possible non-equivalent binding sites for the adsorption of SO_2 on the $Pd_{43}Au_{12}$ cluster.

Adsorption Configuration		d_{S-M}/ Å	d_{O-M}/ Å	d_{S-O}/ Å	∠O-S-O/ °	Adsorption energy/ eV
Initial	Final					
S_V	-	2.407		1.461, 1.461	118.358	-0.52
S_E	-	2.184		1.456, 1.158	117.498	-0.96
S_VO_E	-	2.244	2.334	1.465, 1.512	114.602	-1.02
S_EO_E	$S_EO_VO_E$	2.257	2.355, 2.158	1.511, 1.522	112.124	-1.41
$S_{B2}O_V$	**-**	2.251, 2.250	2.392	1.458, 1.505	113.644	**-1.72**
$S_{B2}O_E$	-	2.260, 2.258	2.537	1.461, 1.483	115.061	-1.51
$S_VO_EO_E$	-	2.405	2.200,2.201	1.512, 1.513	112.985	-1.13
$S_EO_EO_E$	-	2.257	2.239, 2.237	1.512, 1.513	111.530	-1.39

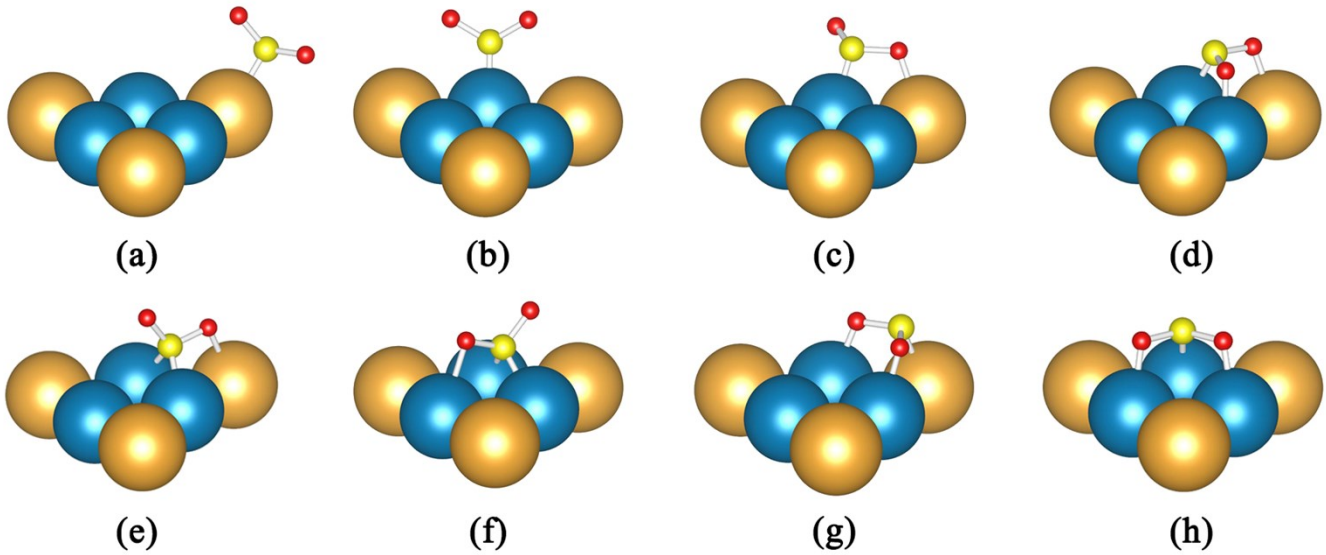

Figure S2 The optimized adsorption configurations at all the possible non-equivalent binding sites for the adsorption of SO_2 on the $Pd_{43}Au_{12}$ cluster.

Table S4 The adsorption energies and geometric data at all the possible non-equivalent binding sites for the adsorption of SO_2 on the $Pd_{13}Au_{42}$ cluster.

Adsorption Configuration		d_{S-M}/ Å	d_{O-M}/ Å	d_{S-O}/ Å	∠O-S-O/ °	Adsorption energy/ eV
Initial	Final					
S_V	-	2.339		1.456,1.455	119.358	-0.55
S_E	-	2.530		1.460,1.459	117.735	-0.32
S_VO_E	-	2.440	2.510	1.464,1.495	116.446	-0.46
S_EO_E	S_E	2.526		1.458,1.471	117.828	-0.32
$S_{B2}O_V$	**-**	2.447,2.460	2.263	1.460,1.525	113.050	**-0.67**
$S_{B2}O_E$	$S_{B2}O_V$	2.466,2.463	2.253	1.460,1.525	112.791	-0.66
$S_VO_EO_E$	-	2.432	2.455,2.428	1.484,1.505	113.631	-0.51
$S_EO_EO_E$	S_E	2.525		1.460,1.459	117.686	-0.32

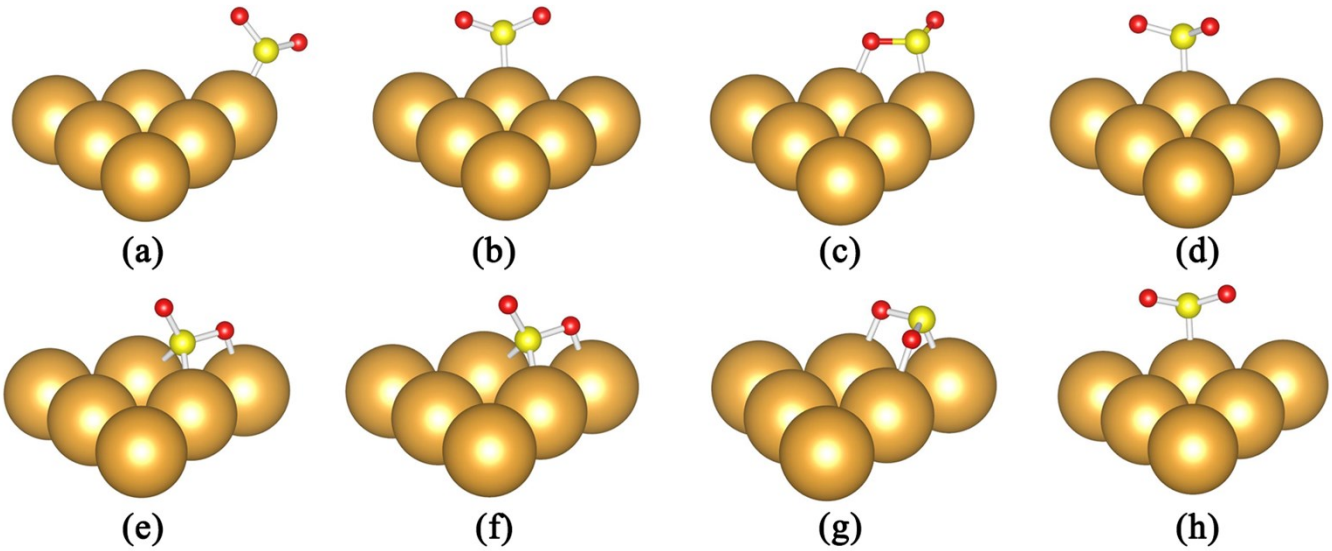

Figure S3 The optimized adsorption configurations at all the possible non-equivalent binding sites for the adsorption of SO_2 on the $Pd_{13}Au_{42}$ cluster.

Table S5 The adsorption energies and geometric data at all the possible non-equivalent binding sites for the adsorption of SO_2 on the Au_{55} cluster.

Adsorption Configuration		d_{S-M}/ Å	d_{O-M}/ Å	d_{S-O}/ Å	∠O-S-O/ °	Adsorption energy/ eV
Initial	Final					
S_V	-	2.432		1.456,1.456	118.864	-0.43
S_E	-	2.497		1.462,1.460	117.564	-0.37
$S_{B2}O_V$	**-**	2.499,2.505	2.391	1.460,1.507	114.274	**-0.96**
$S_{B2}O_E$	**$S_{B2}O_V$**	2.502,2.502	2.358	1.459,1.507	113.896	**-0.99**
$S_VO_EO_E$	S_V	2.427		1.457,1.457	118.386	-0.44
$S_EO_EO_E$	-	2.491	2.434,2.417	1.495,1.497	113.792	-0.73

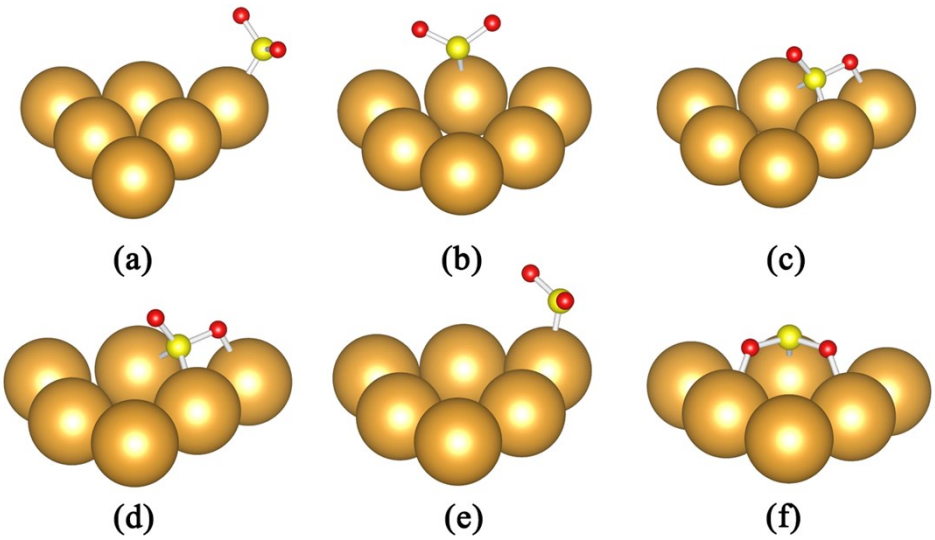

Figure S4 The optimized adsorption configurations at all the possible non-equivalent binding sites for the adsorption of SO_2 on the Au_{55} cluster.

Table S6 The adsorption energies and geometric data at all the possible non-equivalent binding sites for the adsorption of SO_3 on the Pd_xAu_{55-x} (x=0, 13, 43, 55) cluster.

	Adsorption Configuration		d_{S-M}/ Å	d_{O-M}/ Å	d_{S-O}/ Å	E_{ads}/ eV
	Initial	Final				
Pd_{55}	$O_VO_EO_E$	**$S_VO_EO_E$**	2.219	2.172,2.184	1.455,1.519,1.519	**-1.93**
	$O_EO_EO_E$	$S_EO_EO_E$	2.224	2.219,2.241	1.453,1.517,1.521	-1.71
$Pd_{43}Au_{12}$	$O_VO_EO_E$	**$S_VO_EO_E$**	2.334	2.121,2.121	1.448,1.527,1.527	**-1.85**
	$O_EO_EO_E$	$S_EO_EO_E$	2.239	2.282,2.282	1.455,1.505,1.505	-1.53
$Pd_{13}Au_{42}$	**$O_VO_EO_E$**	-		2.132,2.213,2.206	1.544,1531,1.532	**-1.37**
	$O_EO_EO_E$	-		2.226,2.242,2.216	1.532,1.529,1.534	-0.65
Au_{55}	**$O_VO_EO_E$**	-		2.138,2.155,2.174	1.533,1.530,1.528	**-1.56**
	$O_EO_EO_E$	-	2.372	2.266,2.267	1.453,1.511,1.511	-1.25

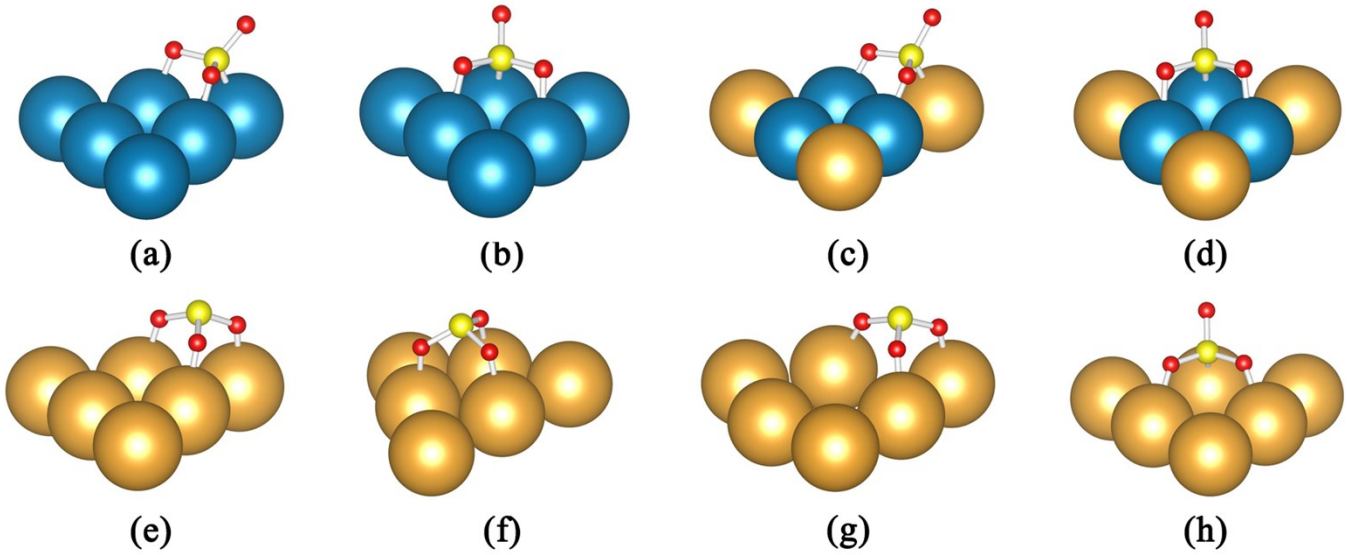

Figure S5 The optimized adsorption configurations at the possible non-equivalent binding sites for the adsorption of SO_3 on the Pd_xAu_{55-x} (x=0, 13, 43, 55) cluster, (a, b) for Pd_{55}, (c, d) for $Pd_{43}Au_{12}$, (e, f) for $Pd_{13}Au_{42}$ and (g, h) for Au_{55}, respectively.

Table S7 The adsorption energies and geometric data at the most favorable binding sites for the adsorption of SO_4 on the Pd_xAu_{55-x} (x=0, 13, 43, 55) cluster.

	Adsorption Configuration	d_{O-M}/ Å	d_{S-O}/ Å	E_{ads}/ eV
Pd_{55}	$O_V O_E O_E$	2.044,2.093,2.088	1.438,1.533,1.520,1.522	-4.76
$Pd_{43}Au_{12}$	$O_V O_E O_E$	2.151,2.077,2.080	1.439,1.521,1.527,1.526	-4.45
$Pd_{13}Au_{42}$	$O_V O_E O_E$	2.111,2.201,2.190	1.440,1.541,1.519,1.520	-4.01
Au_{55}	$O_V O_E O_E$	2.125,2.108,2.165	1.439,1.525,1.530,1.515	-4.29

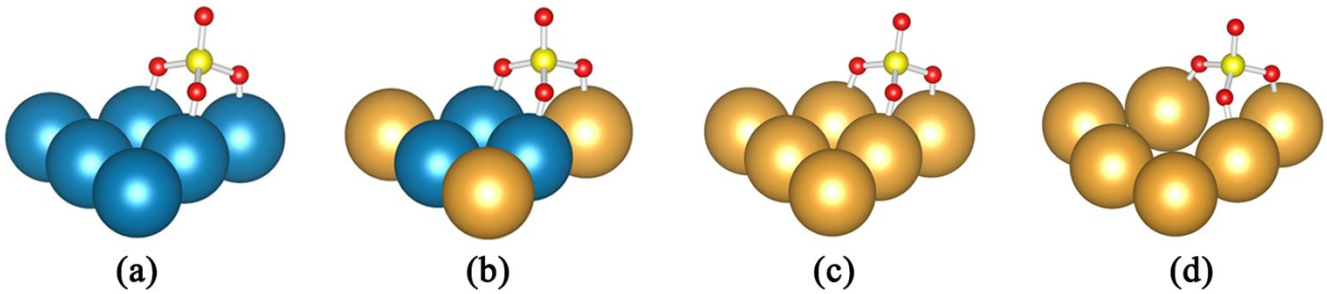

Figure S6 The optimized adsorption configurations at the possible non-equivalent binding sites for the adsorption of SO_4 on the Pd_xAu_{55-x} (x=0, 13, 43, 55) cluster, (a) for Pd_{55}, (b) for $Pd_{43}Au_{12}$, (c) for $Pd_{13}Au_{42}$ and (d) for Au_{55}, respectively.

Table S8 The adsorption energies and geometric data at the most favorable binding sites for the adsorption of O_2 on the Pd_xAu_{55-x} (x=0, 13, 43, 55) cluster.

	Adsorption Configuration		d_{O-M}/ Å	d_{O-O}/ Å	E_{ads}/ eV
	Initial	Final			
Pd_{55}	**O_VO_{B2}**	-	1.966,2.115,2.112	1.379	**-1.62**
	O_VO_E	-	1.967,1.991	1.350	-1.52
$Pd_{43}Au_{12}$	**O_VO_{B2}**	-	2.140,2.109,2.106	1.369	**-1.21**
	O_EO_E	-	2.011,2.012	1.338	-1.20
$Pd_{13}Au_{42}$	**O_VO_{B2}**	-	2.085,2.298,2.308	1.390	**-0.45**
	O_V	-	2.176	1.280	-0.36
Au_{55}	O_VO_{B2}	**O_VO_E**	2.179,2.148	1.328	**-0.43**
	O_EO_E	-	2.290,2.328	1.298	-0.41

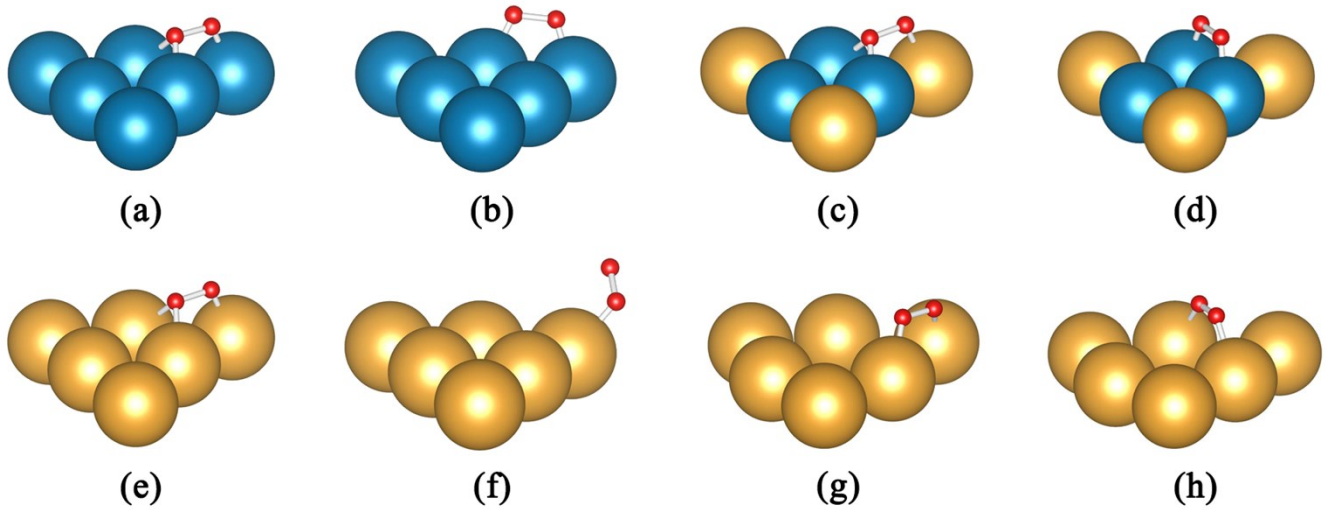

Figure S7 The optimized adsorption configurations at the possible non-equivalent binding sites for the adsorption of O_2 on the Pd_xAu_{55-x} (x=0, 13, 43, 55) cluster, (a, b) for Pd_{55}, (c, d) for $Pd_{43}Au_{12}$, (e, f) for $Pd_{13}Au_{42}$ and (g, h) for Au_{55}, respectively.

Table S9 The adsorption energies and geometric data at the most favorable binding sites for the adsorption of CO on the Pd_xAu_{55-x} (x=0, 13, 43, 55) cluster.

	Adsorption Configuration		d_{C-M}/ Å	d_{C-O}/ Å	E_{ads}/ eV
	Initial	Final			
Pd_{55}	**C_H**	-	2.056,2.043,2.047	1.199	**-2.39**
	C_F	-	2.057,2.056,2.056	1.200	-2.33
$Pd_{43}Au_{12}$	C_H	C_F	2.065,2.062,2.065	1.197	**-2.33**
	C_F	-	2.065,2.065,2.064	1.197	-2.30
$Pd_{13}Au_{42}$	**C_V**	-	1.932	1.154	**-1.25**
	C_E	-	1.972	1.152	-0.80
Au_{55}	C_H	**C_{B2}**	2.134,2.136	1.178	**-1.09**
	C_F	-	2.296,2.246,2.275	1.185	-0.88

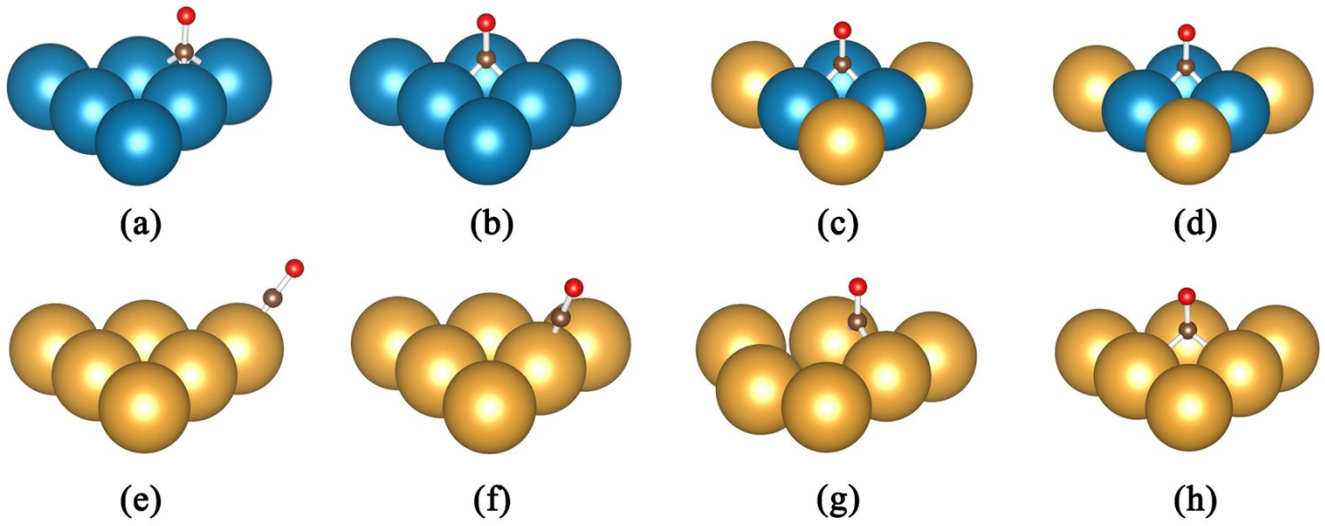

Figure S8 The optimized adsorption configurations at the possible non-equivalent binding sites for the adsorption of CO on the Pd_xAu_{55-x} (x=0, 13, 43, 55) cluster, (a, b) for Pd_{55}, (c, d) for $Pd_{43}Au_{12}$, (e, f) for $Pd_{13}Au_{42}$ and (g, h) for Au_{55}, respectively.

Table S10 Bader charge analysis (in the unit e^-) of the core and shell atoms on Pd_xAu_{55-x} (x=0, 13, 43, 55) cluster.

	Pd_{55}	$Pd_{43}Au_{12}$	$Pd_{13}Au_{42}$	Au_{55}
Core	-0.91	-1.03	-1.23	-1.10
Shell-Pd	+0.91	-0.93		
Shell-Au		+1.96	+1.23	+1.10

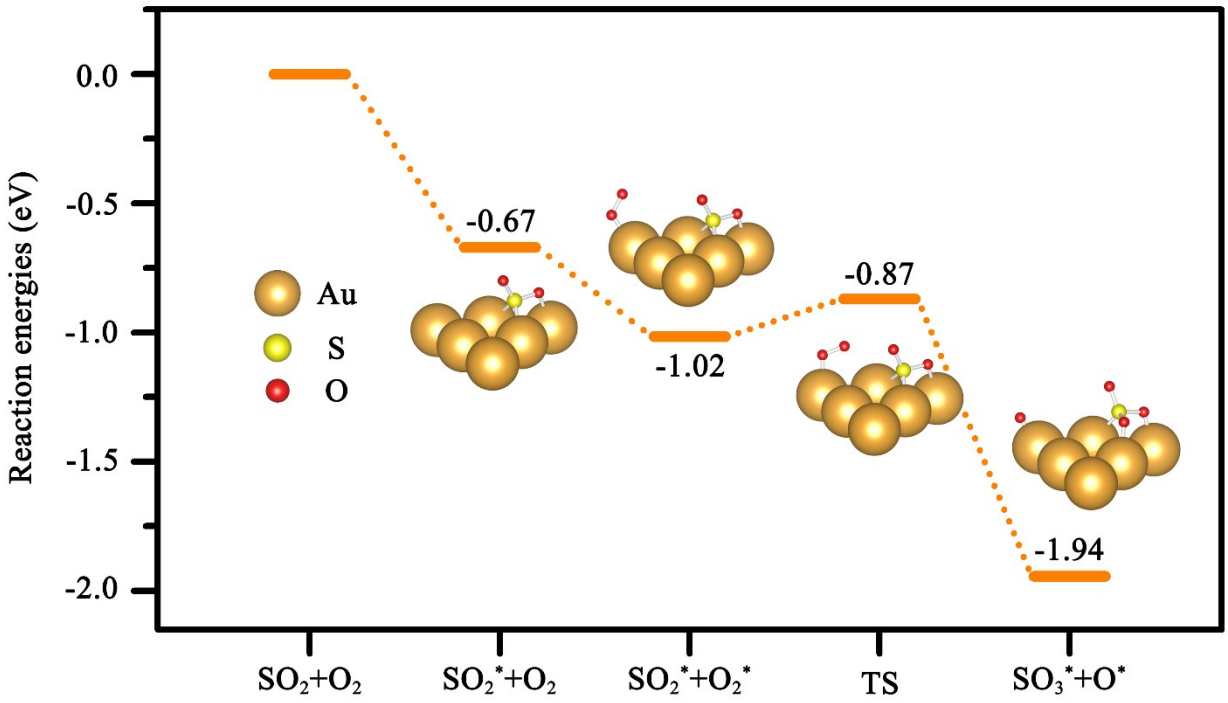

Figure S9 Reaction energy profile and configurations for SO_2 oxidation on $Pd_{13}Au_{42}$ nanoparticle.

Table S11 The adsorption energies and geometric data for the adsorption of SO_2 at the H site on the $M_{13}@Au_{42}$ (M=Ni, Cu, Pd, Ag, Pt) cluster and the d-band center (ε_d) of surface atoms and the core-shell energy (E_{cs}) of M@Au. The E_{ads}, E_{cs} and ε_d in the unit of eV, bond length in Å, and bond angle in °.

	Ni@Au	Cu@Au	Pd@Au	Ag@Au	Pt@Au
E_{ads}	-0.18	-0.44	-0.67	-1.04	-0.62
R_{Au-S}	2.506,2.514	2.498,2.501	2.447,2.460	2.495,2.495	2.447,2.456
R_{Au-O}	2.392	3.109	2.263	2.331	2.345
R_{S-O}	1.457,1.505	1.461,1.466	1.460,1.525	1.459,1.510	1.460,1.507
∠O-S-O	115.078	117.071	113.050	113.625	114.279
Electronegativeity	1.91	1.90	2.20	1.93	2.28
E_{cs}	-0.37	-0.35	-0.34	-0.29	-0.40
ε_d	-3.13	-3.01	-2.87	-2.74	-2.89

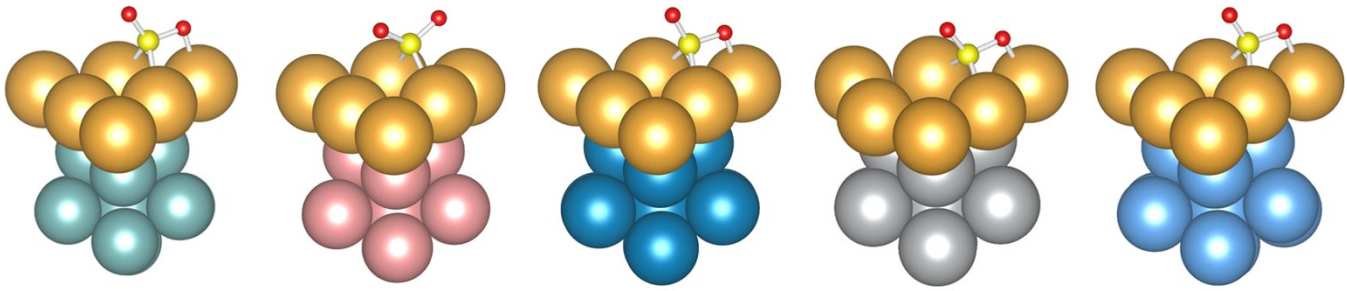

Figure S10 The optimized adsorption configurations for the adsorption of SO_2 at the H binding sites on the Ni@Au (a), Cu@Au (b), Pd@Au (c), Ag@Au (d), and Pt@Au (e), respectively.

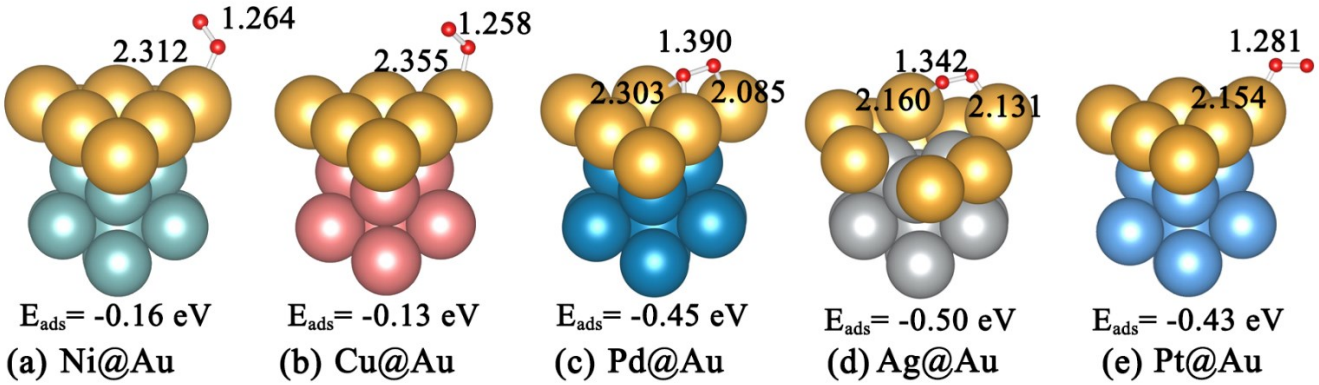

Figure S11 The optimized adsorption configurations and adsorption energies for O_2 on the Ni@Au (a), Cu@Au (b), Pd@Au (c), Ag@Au (d), and Pt@Au (e), respectively. The bond length information is labeled in the unit of Å.

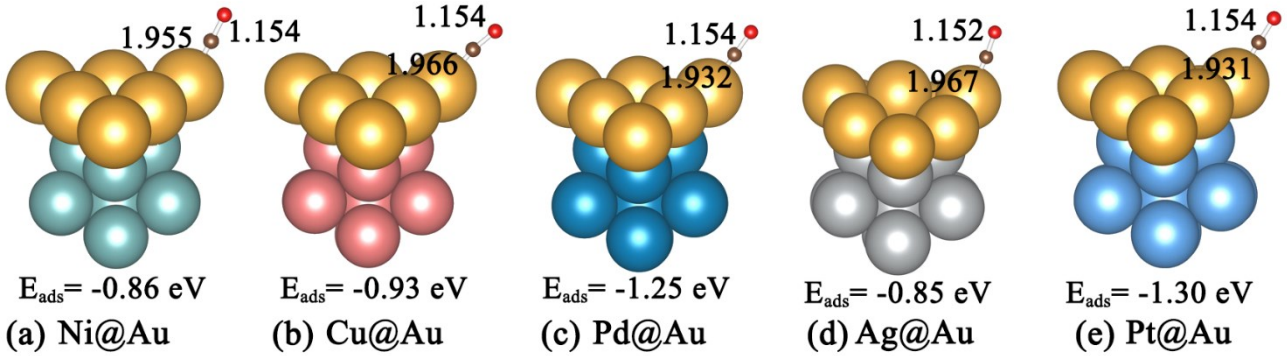

Figure S12 The optimized adsorption configurations and adsorption energies for CO on the Ni@Au (a), Cu@Au (b), Pd@Au (c), Ag@Au (d), and Pt@Au (e), respectively. The bond length information is labeled in the unit of Å.

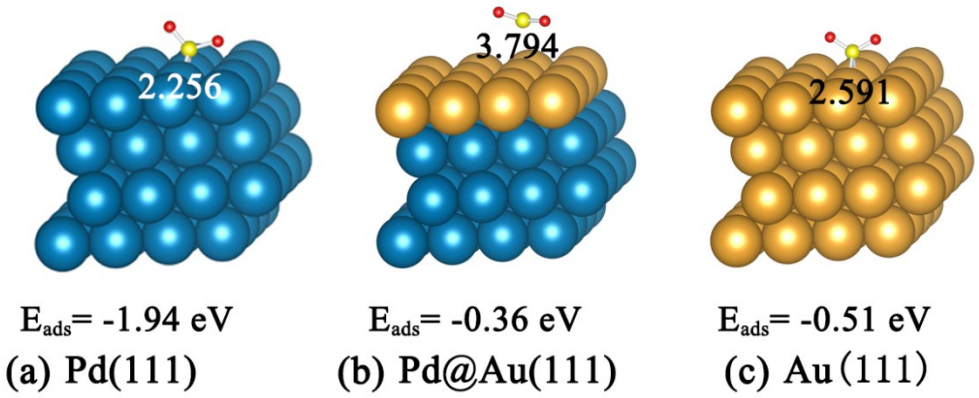

Figure S13 The optimized adsorption configurations and adsorption energies for SO_2 on the Pd(111) (a), Pd@Au(111) (b), and Au(111) (c), respectively. The bond length information is labeled in the unit of Å. For the surface calculations, the *p*(4 × 4) supercell with four-layer atoms was applied, and the bottom two layers were fixed. The vacuum thickness is more than 15 Å perpendicular to the slab surface.

Information for $Pd_{27}Au_{28}$

The most stable configuration of the $Pd_{27}Au_{28}$ nanocluster (Pd:Au ratio is approximately 1:1) is selected using the Monte Carlo simulation and further calculated the relative adsorption information upon SO_2, O_2, and CO. The screened $Pd_{27}Au_{28}$ with Pd as core and Au occupied all surface vertex sites, the rest of Pd and Au atoms random at surface edge sites (Fig. S14a). The LET facets are divided into two types, one has an edge Pd atom on the surface (F1), the other has two edge Pd atoms (F2). The adsorption configurations of SO_2, O_2, and CO on the two type facets and corresponding adsorption energies are shown in Fig. S14. The adsorption energies for $Pd_{27}Au_{28}$ are between which for $Pd_{43}Au_{12}$ and $Pd_{13}Au_{42}$. Meanwhile, the data of $Pd_{27}Au_{28}$ fit the relationship between the SO_2 adsorption energy and the calculated *d*-band center of shell atoms (Fig. S15).

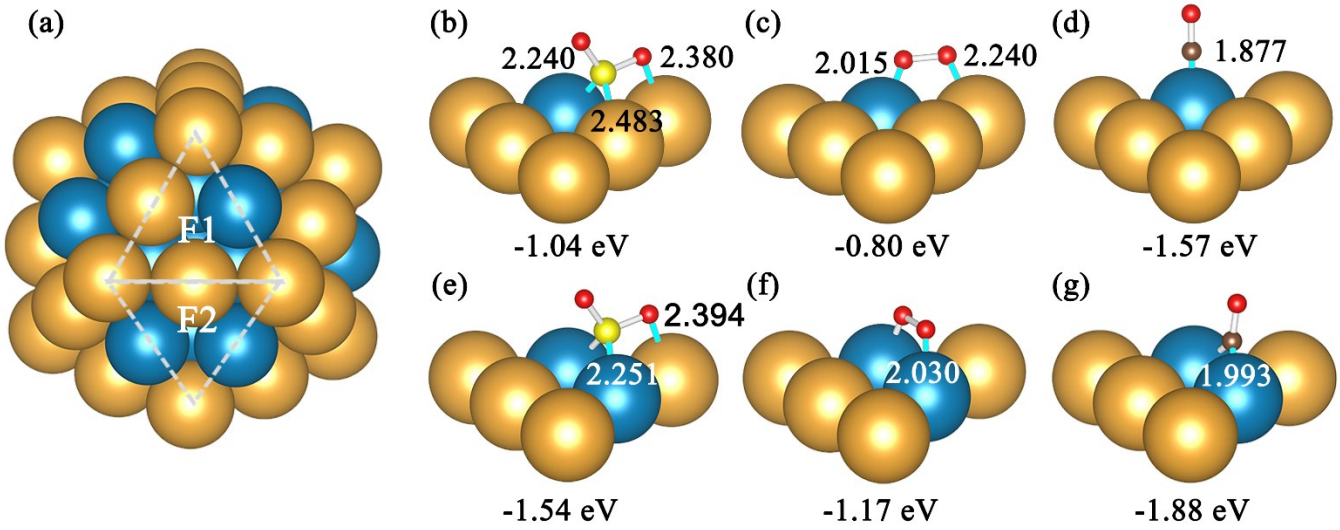

Figure S14 The accepted configurations of the icosahedral $Pd_{27}Au_{28}$ with two types of LET facets (F1 and F2) (a) and the adsorption configurations of SO_2, O_2, and CO on F1 (b-d) and F2 (e-g), respectively. The adsorption energy data is labeled below the structural picture and the bond length information (in the unit of Å) is labeled in color cyan.

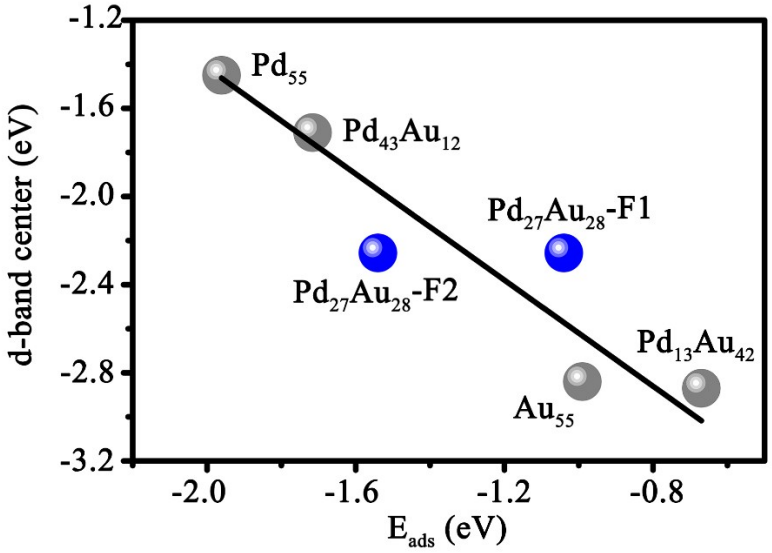

Figure S15 The relationship between the SO_2 adsorption energies and the calculated *d*-band centers of the shell atoms for the Pd_{55}, $Pd_{43}Au_{12}$, $Pd_{27}Au_{28}$, $Pd_{13}Au_{42}$, and Au_{55} nanoparticles.

References

s1. Zhou, X. W.; Johnson, R. A.; Wadley, H. N. G., Misfit-energy-increasing dislocations in vapor-deposited CoFe/NiFe multilayers. *Phys. Rev. B* **2004,** *69* (14), 144113.

s2. Shan, B.; Wang, L.; Yang, S.; Hyun, J.; Kapur, N.; Zhao, Y.; Nicholas, J. B.; Cho, K., First-principles-based embedded atom method for PdAu nanoparticles. *Phys. Rev. B* **2009,** *80* (3), 035404.

s3. Shan, B.; Wang, L.; Yang, S.; Hyun, J.; Kapur, N.; Zhao, Y.; Nicholas, J. B.; Cho, K., Erratum: First-principles-based embedded atom method for PdAu nanoparticles [Phys. Rev. B 80, 035404 (2009)]. *Phys. Rev. B* **2014,** *89* (15), 159903.

s4. Marchal, R.; Genest, A.; Krüger, S.; Rösch, N., Structure of Pd/Au Alloy Nanoparticles from a Density Functional Theory-Based Embedded-Atom Potential. *J. Phys. Chem. C* **2013,** *117* (42), 21810-21822.